



Design, fabrication and testing of an electrical cell stimulation and recording apparatus (ECSARA) for cells in electroculture



Sara Abasi^{a,b}, John R. Aggas^{a,b}, Naren Venkatesh^{a,c}, Iris G. Vallavanatt^a, Anthony Guiseppi-Elie^{a,b,c,d,e,*}

^a Center for Bioelectronics, Biosensors and Biochips (C3B), Department of Biomedical Engineering, Texas A&M University, College Station, TX, 77843, USA

^b Department of Biomedical Engineering, Texas A&M University, College Station, TX, 77843, USA

^c Department of Electrical and Computer Engineering, Texas A&M University, College Station, TX, 77843, USA

^d Department of Cardiovascular Sciences, Houston Methodist Institute for Academic Medicine and Houston Methodist Research Institute, 6670 Bertner Ave., Houston, TX, 77030, USA

^e ABTECH Scientific, Inc., Biotechnology Research Park, 800 East Leigh Street, Richmond, VA, 23219, USA

ARTICLE INFO

Keywords:

Electroculture
EIS
Electric field
Proliferation
HUVECs

ABSTRACT

A new dual-function electrical cell stimulation and recording apparatus (ECSARA) for simultaneously electrically stimulating cellular behavior within programmed stand-off electric fields (EFs) and monitoring cellular responses via AC electrical impedance spectroscopy (EIS) is reported. ECSARA is designed to have a footprint similar to that of a common 24-well cell culture plate within which each well is electrified via a pair of opposing planar titanium electrodes, within the cover (0.10 cm²) and base (0.50 cm²) of each well. Porous cell culture inserts established a 3-D milieu for bathing cells while keeping them away from unfavorable fields and forces in the vicinity of the electrodes. ECSARA was tested for its temporal stability, well-to-well variability, and responses in different media. EF modeling showed the field strength to be uniform in the subtending plane of the insert and the magnitude to be influenced by the porosity of the insert membrane. HUVECs were exposed to EF (162 mV/mm at 1.2 Hz) and monitored with standard viability Blue assay and EIS with equivalent circuit modeling. During the first 24 h, the viability (population) of EF-stimulated cells was smaller than non-stimulated control (0.8) but after 72 h they outnumbered the control (1.2) indicating that stimulation initially inhibited growth but resulted in eventual adaptive proliferation. EIS monitoring showed an increase in R_{cell} of EF stimulated and control HUVECs after 54 h and 78 h, respectively. This was in accord with viability data that showed faster growth of EF-stimulated HUVECs. Confluence was confirmed by VE-cadherin staining. The potential to explore the stimulatory influences of electric fields on cellular processes in tissue and regenerative engineering is now easily possible.

1. Introduction

Potential of cellular behavior under the influence of mild, sustained and discerning electric fields (EFs) has been a noble cause of much research (Kloth, 2005; Robinson, 1985; Yamada et al., 2007). The need for improved understanding of the physiological response of living cells grown in culture under the influence of such fields necessitates development of systems for the simultaneous application of EFs and recording of cellular responses. The nascent production of electrochemicals, locally produced changes in biochemical activities or

biomolecular fluxes under the influence of an EF is an example of the efficiency of harnessing electrical impulses to treat ailments (Famm et al., 2013). The imposition of an EF induces an ionic current through and around the cells of complex multi-cellular tissues. The ionic flows creates an internal EF in the range of 0.01–2.0 V/cm within tissues (Nuccitelli, 1992) contributing in developmental biology (Hotary and Robinson, 1994; Metcalf and Borgens, 1994) and to the healing (Jaffe and Vanable, 1984; Zhao, 2009) of cells and tissue (Nuccitelli, 2003). The presence of endogenous electric current was first shown in 1843 by Raymond du-Bois who was able to measure micro-Amp level currents

* Corresponding author. Center for Bioelectronics, Biosensors and Biochips (C3B), Department of Biomedical Engineering, Texas A&M University, College Station, TX, 77843, USA.

E-mail addresses: saraabasi@tamu.edu (S. Abasi), jraggas1@tamu.edu (J.R. Aggas), naren_venkatesh@tamu.edu (N. Venkatesh), irisv@tamu.edu (I.G. Vallavanatt), guiseppi@tamu.edu (A. Guiseppi-Elie).

<https://doi.org/10.1016/j.bios.2019.111793>

Received 19 August 2019; Received in revised form 14 October 2019; Accepted 17 October 2019

Available online 20 October 2019

0956-5663/© 2019 Elsevier B.V. All rights reserved.

directly from a cut made to his own finger (du Bois-Reymond, 1843). The electrical gradient that occurs as a result of injury has been explored in detail and was shown to be of primary concern in healing (Balint et al., 2013; McCaig et al., 2005; Vanhaesebroeck, 2006). The effective roles of passive electrical cues (Abasi et al., 2019) and external endogenous electrical fields (EF) *in-vivo* prompted the use of electrical stimulation (ES) *in-vitro*, both to better understand the molecular pathways through which EFs affect cellular process as well as applying such cues as a tool to control and guide cellular response, e.g. differentiation (Yamada et al., 2007). This premise has been addressed by developing devices, systems and setups for electrical stimulation (ES), of *in-vivo* range, in a controlled manner to the cells in culture, *in-vitro*. The application of ES has been associated with concomitant heat generation, local pH disruption, accumulation of chemical components (polarization) and possible chemical reactions in the media (Brunner and Turner, 1977; Huang et al., 2001; Song et al., 2007). Electrification systems have been developed over the years to address the forgoing named issues as well as personalize the system for specific application (Mobini et al., 2016; Tandon et al., 2008; Xiong et al., 2015). Providing a means to deliver electrical signals *in-vivo* is beneficial in other areas including development of electrocuring bioadhesives where electric potential is used to initiate the crosslinking of monomers (Gan et al., 2019; Ping et al., 2015).

One of the early approaches to apply an EF was to use Ag/AgCl electrodes through agar salt bridges. This approach used reversible, separated electrodes such that the inherently harmful bi-products of electrification (e.g. reactive oxygen species, free silver ions, or wild shifts in local pH) were made as far away from the living cells as possible (Poo and Robinson, 1977). More recently, Xiong et al. developed an agar salt bridge cell stimulation platform capable of applying DC and square waves at multiple frequencies in a 6-well system (Xiong et al., 2015). While effective, there are some inherent limitations including possibility of contamination, limitation of stimulating signals, duration of the applied field and recording of an impedimetric response were not addressed. Vunjak-Novakovic's group developed a system consisting of two parallel carbon electrodes in a 6 mm petri dish for stimulating cells within a 3-D construct (Tandon et al., 2008). Carbon was selected over traditional metals such as platinum or gold as it showed the highest charge transfer resistance in biological studies (Tandon et al., 2006). In this setup, the two rod electrodes were placed on either side of the cell growing plane. The uniformity of EF between the two electrodes and the field strength delivered to the cells are questionable and dependent on the shape and size of electrodes as well as the scaffold where the cells were cultured. Mobini et al. reported the development of a system which is a simple practical modification of a common 6-well cell culture plate which provides a means of running multiple samples under analogous conditions, again, the electrode placement was similar to the previously developed carbon electrode system, rendering EF uniformity questionable (Mobini et al., 2016). Other suggested and developed setups are mostly based on similar electrode configurations. Among these are the 2.5 cm separated coplanar pair of carbon electrodes to deliver DC and pulse signals to HUVEC cells (Yuan et al., 2014), the Independently Addressable Interdigitated Microsensor Electrodes (IAIMEs) fashioned from gold (IAIME Au), platinum (IAIME Pt) or indium tin oxide (IAIME ITO) of ABTECH Scientific Inc., a similarly configured coplanar arrangement of 5, 10, 15 or 20 μm line and spaced electrodes for the study of cell mobility and migration via electrical impedance (Bieberich and Guiseppi-Elie, 2004), the Biomet® OrthoPak® Non-invasive Bone Growth Stimulator to improve bone healing rates (Griffin and Bayat, 2011), and C-DISH™ launched by IONOPTIX to apply pulse electric fields to cardiomyocytes (Fujita et al., 2007). Despite promising results from a wide range of electrode configurations and patterns of stimulation, the field of electrified cell stimulation still lacks a single system for doing multiple simultaneous experiments using various stimulation wave forms with simultaneous interrogation.

Another entirely different approach in electrophysiology is to use the

electrical properties of cells as a real-time tool for monitoring cellular processes pioneered by Giaeffer and Keese, 1984 (Giaeffer and Keese, 1984). Impedance, the opposition that a system presents to a current when a voltage is applied, has been employed as a meaningful parameter to describe cellular response. Electrical impedance spectroscopy (EIS), the application of a spectrum of interrogating voltage frequencies, is a powerful though non-specific tool that is widely used to study the performance of neural electrodes (Williams et al., 2007), organoid bodies in organ-on-a-chip models (Zhang et al., 2017), and in drug screening (Adcock et al., 2018). The power of the EIS technique is found in the application of the principles of electrostatics to the dynamics of cellular behavior (cell mobility, tight junction formation, ion channel activity, etc.) and sub-cellular components (membrane permeability, inclusion bodies, polarity of the cells, directional alignment, etc.) that appear in the resultant complex impedance. EIS data can be analyzed with equivalent circuit models as simple as the Randles model or more complex models to continuously study cellular behavior (Justin et al., 2009). Lo and Ferrier applied mathematical equations to the experimental data to model the flow of electrical current into and between the cells seeded on ECIS (Electric Cell-substrate Impedance Sensing), the biosensor developed by Giaeffer and Keese, which was later commercialized by Applied Biophysics (Lo and Ferrier, 1998; Lo et al., 1995). Another commercially available system is the impedance-based real-time cell analyzer (RTCA) system by ACEA Biosciences. This system uses transmission line impedance to monitor changes in cellular impedance behavior (Xing et al., 2005). The cellZscope launched by nanoAnalytics is specialized for measuring the transepithelial/- endothelial electrical impedance/resistance of the cells (TEER) (Wegener et al., 2004). A pair of stainless-steel parallel electrodes were used to measure the impedance of the cell layer formed on a cell culture insert. Applied Biophysics subsequently offered a very similar device for TEER measurement called TEER 24.

In this report, a dual-function Electrical Cell Stimulation and Recording Apparatus (ECSARA) was designed, fabricated, programmed and applied with the aim of addressing deficiencies of currently available systems while demonstrating improved performance and reliability. Furthermore, while the available systems were developed to perform either as a bioreactor or a monitoring device, the current system of this study combines the two paradigms to allow concomitant electrical stimulation using variable wave forms and duty cycles in bioreactor mode while periodically and systematically in a fully programmed manner, measuring the complex impedance of the cells or organoids under examination. Thus, ECSARA is a tool to apply ES to cells in 3D culture on porous inserts as well as 3-D organoids while monitoring the cellular behavior through their electrical impedance.

2. Electrical cell stimulation and recording apparatus (ECSARA)

2.1. Design criteria

Applying an electric potential between two infinitely wide ideal electrodes within a vacuum induces a collimated uniform EF between them with a field strength of $E = V/d$, where E , V , and d stands for EF strength (V/m), applied voltage (V) to the electrodes, and distance (m) between the two electrodes, respectively. The forgoing establishes a uniform gradient between the idealized electrodes. For real electrodes subtending real cell culture media, the distribution of the electrical field is not uniform, and the gradient is not linear. The ECSARA seeks to apply a uniform EF to all cells with an expectation that all cells experience the same EF. This was achieved by placing two opposing disk electrodes with their disk faces parallel to each other and on either side of the plane of cell culture. This electrode configuration ensures that all the cells in culture were exposed to a uniform, consistent field. The strength of the effective electric field (E) between the electrodes is governed by Gauss' law: $E = \sigma / (k\epsilon_0)$, where σ is the sheet charge density (C/m^2), k is the dielectric constant, and ϵ_0 is the permittivity in vacuum ($8.85 \times 10^{-12} \text{ F}$ /

m). With the promise of keeping the cells away from direct contact with electrodes, hanging cell culture inserts were used to suspend the cells approximately equidistantly between the two electrodes. These inserts provide a specific footprint for cell culture to accommodate either direct cell seeding or as a substrate for scaffolds/tissues/organoids between the electrodes as well as enabling simple transfer of cultures from the ECSARA for imaging or other evaluation purposes. There exist multiple options for insert footprint (e.g. $\phi = 0.65$ cm or $A = 0.3$ cm²), pore size (0.4–8.0 μ m) and membrane material (polyethylene terephthalate, polytetrafluoroethylene, mixed cellulose esters or polycarbonate). In order to accommodate the standard commercial insert, the ECSARA electroculture plate was fashioned as the same physical design parameters as a standard 24-well cell culture plate.

2.2. System configuration

The ECSARA system comprised the following four main components: i) the 24-well electroculture plate (base, body, and lid), ii) the interrogation hardware of signal generator, frequency response analyzer, multiplexer unit, computer, and associated cabling, iii) the controlling and data acquisition software, and iv) the data processing and analysis software.

2.2.1. The 24-well ECSARA electroculture plate

The 24-well ECSARA electroculture plate is a modular design, made of a three-part polymeric chamber outfitted with metal electrodes. The chamber consists of three discrete parts: lid, body, and base, all produced from an FDA approved polypropylene (EP42HT-2Med, Tecapro MT, Total Plastics, Fort Wayne, IN). The Tecapro MT meets the USP Class VI requirement which addresses the *in-vivo* cytotoxicity of the material extracts. The chamber was fabricated from a design developed in Solid Works 2018 (Dassult Systems) using CNC machining (Haas Mill G Codes) with an accuracy of 0.0001" (inches). Early designs were produced, inspected and validated by rapid prototyping using a desktop 3-D printer (Stratasys Mojo). All critical external and internal dimensions of the chamber were selected to replicate a common 24-well tissue culture plate. Fig. 1A is an exploded view that shows individual parts and final assembly of the actual electroculture plate. Titanium grade 23 (6AL-4V ELI) (TMS Titanium, Poway, CA) was used for electrodes of each well. The top electrode was sourced as rod stock and cut into discrete lengths and the bottom electrode sourced as sheet stock and cut into plates. Titanium Grade 23 is an alloy that consists of titanium (88.5–91% purity), carbon (0.08% max), nitrogen (0.03% max), oxygen (0.13% max), hydrogen (0.0125% max), vanadium (3.5–4.5%), aluminum (5.5–6.5%), and iron (0.25% max). The electrode system comprised a single rectangular plate (127 × 85 × 33 mm) that served as

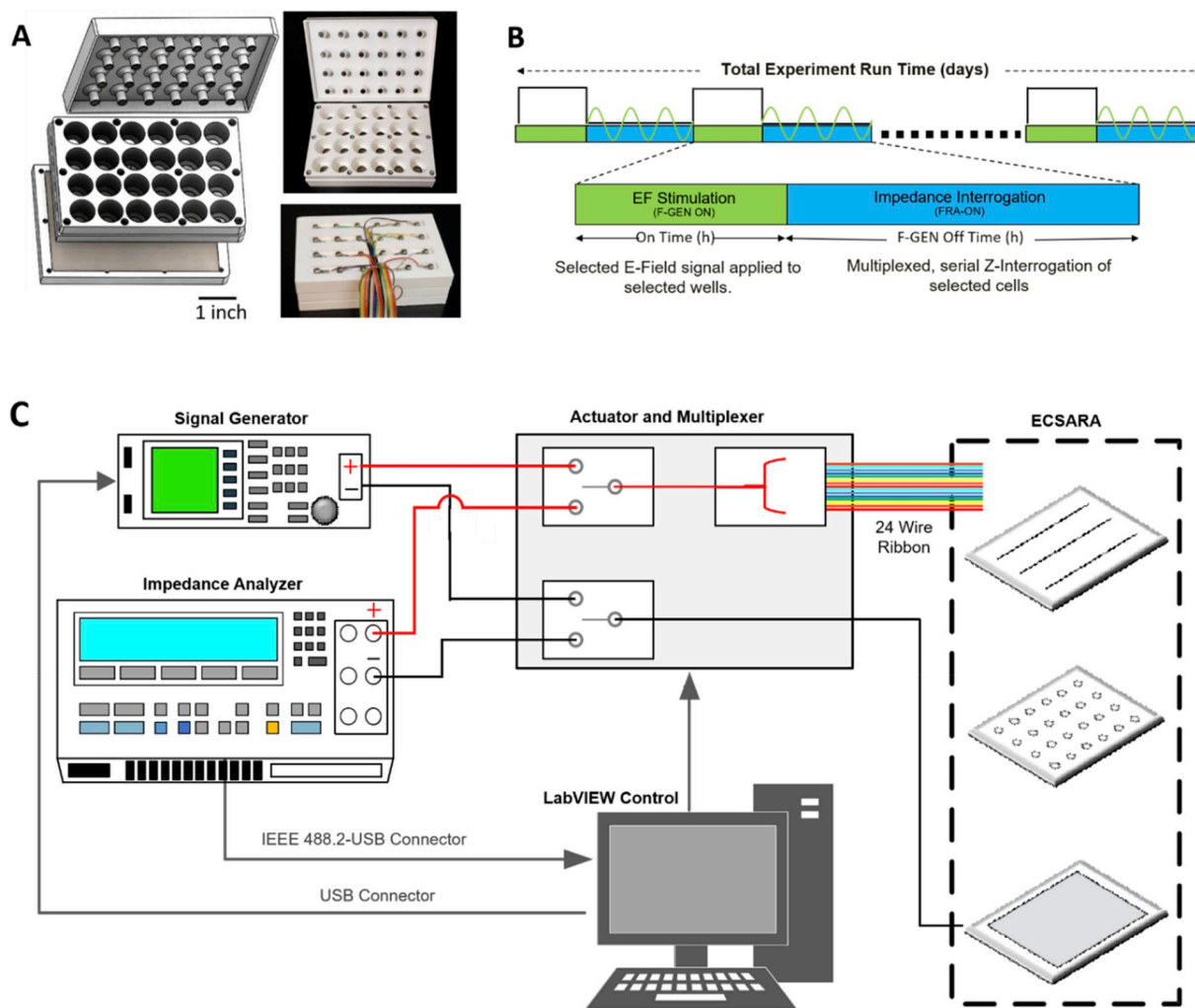


Fig. 1. (A) An exploded schematic and photographs of the ECSARA electroculture plate showing lid, body, and base of the electroculture plate with the photograph of the assembled but opened plate showing top and base electrodes and electrical connections to the top and bottom electrodes. (B) The timeline of the electric field stimulation and impedance interrogation commands used by the software, and (C) Schematic illustration of ECSARA showing the instrumentation control and data acquisition system (hardware).

a common return electrode beneath all 24 wells and 24 opposing, independently addressable rod electrodes ($\phi = 4.78$ mm and $L = 12.44$ mm), each rod corresponded to a single well. The sheet and rod electrodes were mounted within the base and lid, respectively, which kept them separated by 7.4 mm when in place. The independent wells were sealed with medical grade Viton O-rings (Apple Rubber, Lancaster, NY) that were placed beneath each well within a circular groove devised for it which limited the area of the bottom electrode to a disk of 9.91 mm diameter. The rod electrodes were sealed into hollow cylindrical housings that extended downwards from the lid using a cytocompatible, two-component epoxy (EP42HT-2MED clear, MASTER BOND, Hackensack, NJ). The epoxy formed a thin layer around the metallic rods to both secure them into the cylindrical housings and ensure that no fluid could seep between the rod and its housing. Thus, a two-electrode electrification system comprised of $A_1 = 17.95$ mm² (top electrode), $A_2 = 77.08$ mm² (bottom electrode) separated by 7.4 mm was fashioned. The base and body were screwed together with twelve Type 316 stainless steel bolts and nuts, evenly distributed throughout the plate to provide a uniform pressure to the O-rings and thus seal the wells. Electrical connections were provided by a 25-lead flat cable (28G) secured to each of the 24 rods, through a stainless-steel screw (Super-Corrosion-Resistant, 2–56 Thread Size, 1/8" Long) into the head of the rod. The 25th lead served the return electrode.

2.2.2. Interrogation hardware

The interrogation hardware comprised of a signal generator (SDG1025, Siglent, Solon, OH) to deliver electrical cell stimulation, a frequency response analyzer (FRA) (Solartron 1260A, Ametek Inc., Berwyn, PA) to collect EIS data, and a data acquisition/multiplexer unit (34970A, Hewlett Packard, Palo Alto, CA) to multiplex the signal between the generator and FRA as well as sequentially among each individual well of the 24-well electroculture plate. The interrogation hardware was designed so that at any given time, either the signal generator or FRA could be turned on and into use. As shown in Fig. 1C, both working electrodes of the signal generator and FRA were wired to an actuator channel within the multiplexer unit. The output of this actuator was directed to a 24-plex multiplexer, where each output of the multiplexer was directed to one of the 24 rod electrodes located in the cover of the electroculture plate. In a similar fashion, the counter electrodes of both systems were wired to an actuator which was directed to the return sheet electrode. This arrangement allowed the actuators to switch between the signal generator and FRA per need and as programmed. When the signal generator was in use, all 24 channels of the multiplexer were activated, so that an electrical signal could be applied between each of the 24 rod electrodes and the return sheet electrode. When the FRA was in use, each channel of the multiplexer could be sequentially cycled through, allowing for measurement spectra of each individual well.

2.2.3. Controlling and data acquisition software (CDAS)

Custom instrument control and data acquisition software was developed in LabVIEW. The interrogation hardware (signal generator, multiplexer unit, and FRA) communicated via a custom LabVIEW block diagram and Graphical User Interface (GUI) (Fig. 1C). The software was written to execute multiple tasks on a loop over a total experiment runtime (usually several days). A timeline of the commands used by the software is shown in Fig. 1B. Briefly, an electric signal is applied to selected wells of the electroculture plate for a specified time, then upon completion, the signal generator is turned off, the software triggers the multiplex unit to switch over to the impedance analyzer where impedance spectra are measured in a well-by-well manner. The acquired data are exported into excel workbooks and individual ".z" impedance files.

The GUI was created to allow customized experiments, with variability in which (if not all) of the 24 wells would be used in a particular experiment, including parameters of the simulation signal produced by the signal generator, parameters of the impedance analysis, and the total

experiment time. Particularly, the type of signal (square, sinusoidal, triangular, DC), frequency (1 mHz–50 MHz), amplitude (1–20 mV p-t-p) and duty cycle (0–100%) were all programmable. In addition, parameters of the impedance measurements, such as interrogation signal amplitude, frequency window (10 μ Hz - 32 MHz with 0.015 ppm resolution), and number of points to measure per decade were made variable. The FRA can elicit impedance at frequencies as low as 10 μ Hz, however, it should be noted that sampling at low frequencies would be at the cost of losing contributions from fast-occurring events. Consequently, the frequency range for impedance acquisition should be set dependent on the type of important information meant to be captured.

2.3. Data processing

The large volume of recorded data (e.g. up to 30 spectral files per well) over the time course of a five-day electroculture exercise) places unique demands on the data processing component of the system. The data captured in excel workbooks and as individual ".z" impedance files were exported and subjected to equivalent circuit analysis using the Expanded Zfit Matlab script. The customized Expanded Zfit Matlab script was used for large scale equivalent circuit (EQCRT) analysis and was modified to take the recorded data as input and then output the best values of the electrical circuit elements based on "goodness of fit" (χ^2) criteria applied to several candidate models. To be useful, equivalent circuit analysis must be based on models that have a basis in the physical electrochemistry, electrostatics and ionics of the system under examination. Data processing seeks to extract the equivalent circuit elements attributable to the electrochemical and mass transport processes to find the key model parameter representing the device under test (DUT) (Franks et al., 2005). Data processing seeks to extract and ascribe a final membrane resistance (R_{Cell}) and membrane capacitance (Q_{Cell}) attributable to the layer of cells cultured on the cell culture insert between the electrodes. Real-time, temporal complex impedance data acquired in the CDAS module above must therefore be modeled using equivalent circuit modeling and the key model parameter representing R_{Cell} and Q_{Cell} extracted and presented as the desired result.

3. Experimental materials and methods

3.1. Materials

HEPES buffer, PBS buffer, potassium ferrocyanide/potassium ferricyanide [Fe(II)/Fe(III)], Dulbecco's Modified Eagle's Medium (DMEM, high glucose), RPMI-1640 Medium (With L-glutamine and sodium bicarbonate) were obtained from Sigma Aldrich. De-ionized, ultrapure water was collected from a Milli-Q® plus (Millipore Inc.) ultrapure water system. For cell culture studies, primary Human Umbilical Vein Endothelial Cells (HUVECs, neonatal pooled, 200P–05N) were obtained from Sigma-Aldrich and cultured according to the protocol provided by the supplier in Endothelial Cell Growth Medium supplied with 1% Penicillin-Streptomycin (10,000 units penicillin and 10 mg streptomycin/mL, PS) (Sigma-Aldrich). Trypsin-EDTA (0.25% trypsin, 0.02% EDTA) solution, trypsin inhibitor and gelatin were similarly purchased from Sigma-Aldrich. Phosphate-buffered saline (PBS) tablets (Gibco, Thermo Fisher Scientific, Waltham, MA) were dissolved in DI water to prepare 0.01 M (pH 7.4) buffer solution. AlamarBlue™ Cell Viability Reagent, rhodamine-phalloidin and DAPI were purchased from Thermo Fisher Scientific. Anti-VE cadherin antibody conjugated to Alexa Fluor 488® was purchased from Santa Cruz Biotechnology (TX).

3.2. Characterization

3.2.1. Temporal impedimetric behavior and well-to-well variability

To evaluate the temporal behavior of the system as well as variability between the wells, the impedance of 2.0 mL of 0.01 M PBS was measured every 6 h over 5 days at 37 °C in an incubator (VWR 2310 CO₂

Incubator). Impedance measurements were completed using a 20 mV p-p sinusoidal voltage from 10 mHz - 1 MHz. Prior to impedance measurements, the top rod electrodes were mechanically polished with standard polishing kit using 15.0 μm diamond slurry (5 min) followed by 0.05 μm alumina (3 min) (Bioanalytical System, Inc., IN) then thoroughly rinsed in DI water.

3.2.2. Impedimetric behavior of ECSARA using six physiological media

The impedance of 6 different media: DI water, 0.01 M PBS, 0.1 M HEPES, 0.1 M Fe(II)/Fe(III), DMEM, and RPMI were separately evaluated. These media were chosen as they are the most common media used in *in-vitro* cell culture studies. The Fe(II)/Fe(III) system is an electroactive couple often used as a redox probe in biosensor studies. Four wells of the 24-well ECSARA were filled with 2.0 mL of each media and impedance spectra were collected in an incubator at 37 °C using 20 mV p-p sinusoidal voltage over the range 10 mHz–1 MHz.

3.2.3. Contribution of cell-culture insert to impedance

To study the contribution of the cell culture insert to the overall impedance of the electroculture well, 12 polyethylene terephthalate (PET) inserts with pore size of 3.0 μm and pore density of 2×10^6 pores/cm² (Corning, Millipore, MA) were pre-hydrated in 0.01 M PBS and placed within 12 wells of the ECSARA and all the 24 wells were filled with 0.01 M PBS. Impedance measurements were taken under similar conditions as previous tests in the incubator at 37 °C every 6 h for 2 days.

3.2.4. Equivalent circuit analysis

Two equivalent circuit models were used to analyze impedance spectra, the simpler of these, the Randles Equivalent Circuit (R(QR)), comprises a solution/membrane resistance (R_S or R_M) in series with a parallel combination of a charge transfer resistance (R_{CT}) and double layer capacitance (Q_{DL}), thus, ($R_{S/M}(Q_{DL}R_{CT})$) (Sun, 2008) (Yang and Guiseppi-Elie, 2008). A more complex equivalent circuit was developed to better characterize the system in question ($R_S(Q_{OX}R_{OX})(Q_{DL}R_{CT})$) or ($LR_S(Q_{OX}R_{OX})(Q_{DL}R_{CT})$), in which an additional parallel resistance and capacitance is placed in series after the charge transfer resistance and double layer capacitance to signify the resistance and capacitance of the native oxide layer formed on the surface of the titanium alloy electrodes used (R_{OX} , Q_{OX}). The inductance (L) represents the inherent inductive effect of the ribbon cable which was calculated to be on the range $\sim 2 \mu\text{H}$ for the diameter (28G) and length (100 cm) of the cable used for connecting the plate to the measuring device. All circuits were used in analysis to extract either the R_S or R_M . The more complex circuit was used as a model to validate the use of the simpler, less computationally demanding Randles circuit. Equivalent circuit analysis was completed using either ZSimpWin 3.60 (Princeton Applied Research, Oak Ridge, TN) or the customized Expanded Zfit MATLAB script (originally written by Dr. Jean-Luc Delli (2010)).

3.3. Simulation of electric field (EF) distribution within the well

The 3D geometric model was developed in SolidWorks (2018) according to actual dimensions and placement of the electrodes and cell culture insert (Millicell® Hanging Cell Culture Inserts, Millipore, MA). An electrical field and potential simulation was then carried out using 3D-Maxwell in ANSYS as an electrostatic study. The electrostatic analysis assumes the system to be in the low-frequency electromagnetic domain where the displacement currents are negligible and hence neglected. The analysis is based on the assumption that no current exists in any material and objects are either perfect conductors with infinite electric conductivity or perfect insulators with zero electric conductivity. Electrical properties of each material were assigned according to Table 1.

3.4. Implementation of ECSARA in real-time monitoring the effect of electric field on HUVECs

To explore the effect of EF on HUVECs, cells were divided into two groups, EF-stimulated cells and non-EF-stimulated cells or control. The temporal impedance response, metabolic activity via alamarBlue™ assay, and cell morphology via fixation and staining were examined. Cell culture inserts of pore size corresponding to 0.4 μm and pore density of 1×10^8 pores/cm² (12.6% porosity) (Corning, Millipore, MA) were used to culture HUVECs. The inserts were incubated (30 min) with 50 μL of 2 wt% gelatin in PBS and washed three times with PBS prior to cell seeding. HUVECs were cultured to confluency in regular T75 cell culture flask, trypsinized and transferred to inserts at a seeding level of 5×10^4 cells/mL (3.3×10^4 cells/cm²). The viability of cells was determined to be 94% using trypan-blue and hemocytometer prior to seeding. At 6 h post seeding, a pulse of 1.2 V corresponded to electric field of 162 mV/mm at frequency of 1.2 Hz and pulse width of 2 ms was applied to the cells continuously except for the time interrupted for impedance measurement (approximately 45 min every 6 h). Same identical cells were used as control with no exposure to the EF. The impedance of the test and control wells was measured every 6 h at interrogation voltage of 20 mV p-p and within frequency range of 0.01 Hz–1 MHz. The alamarBlue™ assay was performed according to standard protocols. Every 24 h, the media of EF stimulated and control wells was replaced with media containing 10% alamarBlue™ followed by 2 h incubation in the incubator. The absorbance of the media was subsequently measured using a Synergy HT (BioTek Instruments, Inc.). The media containing alamarBlue™ was replaced with regular media after running the assay. For visualization, the cells on an insert were fixed (4% formaldehyde), permeabilized (0.1% Triton x-100), blocked (10% BSA), and stained with anti-VE cadherin antibody conjugated to Alexa Fluor 488®, rhodamine-phalloidin, and DAPI. The membrane was then cut away from the insert and the cells were imaged with an inverted Zeiss fluorescent microscope (Observer Z1).

The EIS data collected prior to seeding (media with insert) were modeled to $R_M(Q_{OX}R_{OX})(Q_{DL}R_{CT})$ to extract the values of those equivalent circuit elements which remain constant in the system. The data collected from continuous EIS measurement following cell seeding were subsequently fitted to $LR_M(Q_{Cell}R_{Cell})(Q_{OX}R_{OX})(Q_{DL}R_{CT})$ keeping the values of L, Q_{DL} , and R_{CT} constant from the fitted model on the data without cells. Q_{Cell} represents the capacitance that the cellular layer introduced to the system due to their charged membrane and R_{Cell} represent the trans-cellular resistance due to tight junction formation between the cells as they form a confluent monolayer and establish a transmembrane resistances.

3.5. Statistical analysis

Outliers, which were defined as values outside the 1.5 interquartile range (IQR) of first and third quartiles were removed. Blocking of data in a randomized complete block design (RCBD) was performed using JMP 13.0 (SAS group) for more meaningful comparison. The means were compared together using a student t-test and p-values < 0.05 were considered significant.

Table 1
Electrical properties of the material components used in the simulation of the electric field.

	Conductivity (S/m)	Relative Permittivity
Titanium	1.82×10^6	1
Polyethylene terephthalate (PET)	1×10^{-15}	3
Polystyrene	1×10^{-16}	2.6
Phosphate buffer saline (PBS)	1	80

4. Results and discussion

4.1. Temporal study and well-to-well variability

Impedance spectra of cells in culture supported on inserts that were measured continually over a six-day period were expected to reveal changes in their trans-membrane permeability, the quality of tight-junctions between and among cells and the overall density of cells. These were expected to manifest as changes to the value of the cell-related circuit elements of an appropriate equivalent circuit model. However, changes in the media pH, redox potential (EH), ion concentration, protein production and protein adsorption onto electrodes are expected to contribute to temporal changes in impedance spectra. These must be distinguished from temporal drift arising from changes to the system itself. System drift was measured as a temporal effect to the resolved solution resistance, R_S , of 0.01 M phosphate buffered saline (PBS) determined every 6 h over 5 days at 37 °C. R_S was calculated by modeling the EIS data using an $R_S(Q_{OX}R_{OX})(Q_{DL}R_{CT})$ model. A randomized complete block design (RCBD) was used by taking the response of the 24 wells as a block. Other than four time points where R_S was significantly different ($p < 0.01$), the magnitude of R_S remained the same over the entire time period. Well-to-well variability was studied from the temporal analysis of R_S , which showed no discernible pattern with time. To evaluate the variation between the wells, R_S for each well was averaged over time. The average of each well was then compared with other wells using RCBD and taking the time as a block. The average R_S of the wells was $37.59 \pm 5.29 \Omega \cdot \text{cm}^2$ with one well that was significantly different ($p < 0.01$) from the rest.

Fig. 2A shows the elements of the $R(QR)(QR)$ equivalent circuit averaged over 24 wells measured at five time points (every 24 h) when the wells contained PBS at 37 °C. Fig. 2B shows the magnitude of R_S for

four randomly selected wells as well as the average of all 24 wells over time. Statistical analysis showed that R_S did not depend on time and the variation did not follow a time-based trend. R_S , solution resistance, was chosen to represent stability of the system as all the events occurring within the solution in this case are counted in this parameter. The pattern of variation suggests that the R_S values extracted from impedance measurements might have been sensitive to some other factor, possibly some environmental factor such as vibration of the work platform and/or electrical noise in the room.

The possibility of using the simpler $R_S(Q_{DL}R_{CT})$ model was evaluated. The χ^2 for $R_S(Q_{DL}R_{CT})$ and $R_S(Q_{OX}R_{OX})(Q_{DL}R_{CT})$ was 0.60 ± 0.09 and 0.50 ± 0.08 , respectively. The results showed that the magnitude of R_S (a parameter of interest) was at maximum 2% different from the values calculated from $R_S(Q_{OX}R_{OX})(Q_{DL}R_{CT})$ and followed the same trend (data not shown). The variation of R_S however was slightly higher for $R_S(Q_{DL}R_{CT})$ compared to the $R_S(Q_{OX}R_{OX})(Q_{DL}R_{CT})$ model, therefore the more complex $R(QR)(QR)$ model was found to be more appropriate for data interpretation.

The titanium alloy used in the system is a commonly used material in biomedical implants, because of the formation of a biocompatible and corrosion resistant passive oxide layer (principally TiO_2) (Tamilselvi et al., 2006). One of the design concerns was that the formation of such an oxide layer would change the temporal electrode characteristics hence affect the impedance. The result of the temporal study indicated that such chemical phenomena did not contribute in the magnitude of solution or membrane resistance in the configuration employed. It was shown by Tamilselvi et al., however, that formation of an oxide layer on Ti-6Al-4V ELI alloy changed the charge transfer resistance and double layer capacitance significantly. In the same study, the formation of a stable passive oxide layer was estimated to occur during 360 h. It should be noted that the cleaning technique that was applied in the mentioned

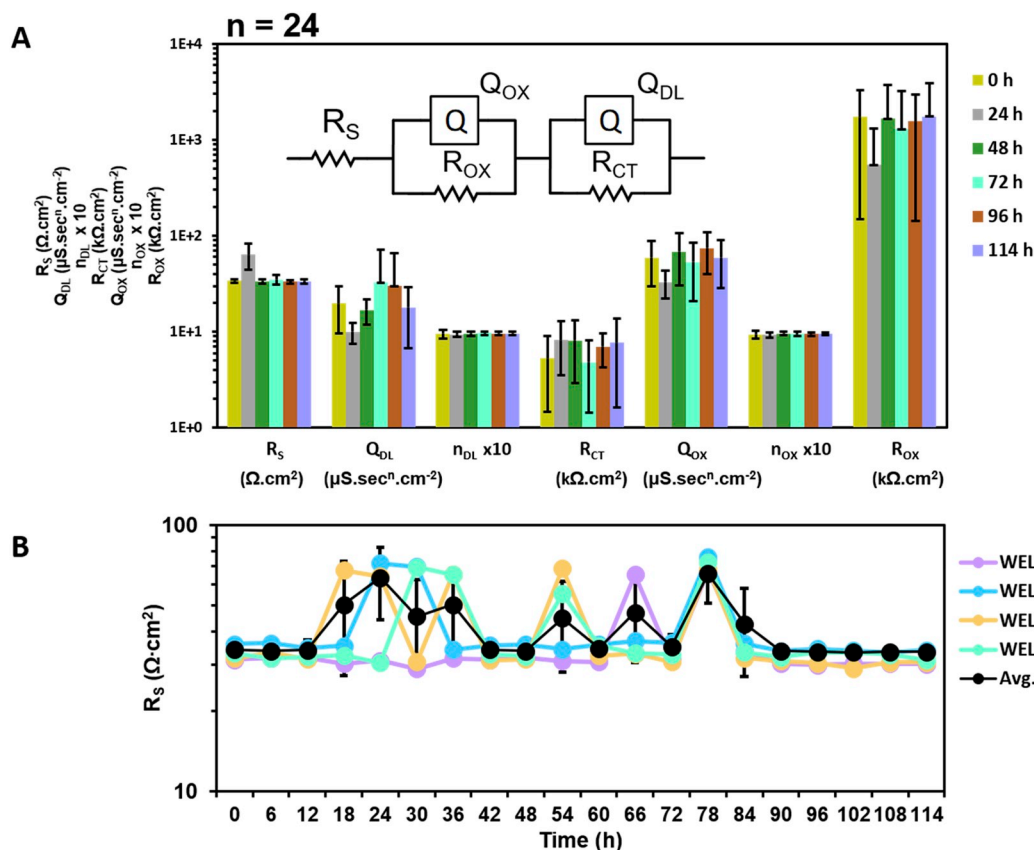


Fig. 2. Results of the temporal and well-to-well variability study showing (A) the result of equivalent circuit analysis of EIS data collected from 0.01 M PBS every 24 h averaged over 24 wells and (B) the changes in magnitude of R_S over 5 days shown for four randomly selected wells and the average of all 24 wells.

study (Tamilselvi et al., 2006) was more aggressive than what was used for ECSARA. In fact, a gentler polishing, that is good enough to clean the electrodes but not completely remove the oxide layer, was preferred in this study in order to have a stable electrode performance. While the presence of an oxide layer increases the charge transfer resistance, there is not a practical way to prevent growth of such a native layer hence the electrodes won't be stable in the case of complete removal. Moreover, the formation of the oxide layer results in the current being delivered capacitively which is a safer way to deliver electrical stimulation to the living specimens. It is for the forgoing reasons that cells were presented in a stand-off configuration on cell culture inserts and not in direct contact with electrodes.

4.2. Characterization of the ECSARA with different media

The difference in the electrolyte strength of the media considerably affected the magnitude of the double layer capacitance, Q_{DL} , and charge transfer resistance, R_{CT} , but was expected to principally affect the magnitude of the solution resistance, R_S . Therefore, to more accurately identify the magnitudes of Q_{DL} , R_{CT} , and R_S , the inductance (L) element, representing the system's cabling, was added to the equivalent circuit model. The results of equivalent circuit LR(QR)(QR) model analysis is summarized in Fig. 3. The magnitude of inductance was calculated to be $9 \pm 2 \mu\text{H}\cdot\text{cm}^{-2}$ for different media which was a very close approximation to what theoretically calculated for the specific ribbon cable used in this system. The size of Q_{DL} was calculated to be $\sim 0.5 \text{ nS}\cdot\text{sec}^n\cdot\text{cm}^2$ for DI water and HEPES (weak electrolyte) and $\sim 20 \mu\text{S}\cdot\text{sec}^n\cdot\text{cm}^{-2}$ for PBS, DMEM, RPMI, and Fe(II)/Fe(III) (redox electrolyte). Higher ion content in the later groups resulted to larger double layer capacitance (Brown et al., 2016). The capacitance and resistance attributed to the oxide-laden interface were retained in the range of $\sim 12 \mu\text{S}\cdot\text{sec}^n\cdot\text{cm}^{-2}$ and $\sim 4 \text{ M}\Omega\cdot\text{cm}^2$ and were not influenced by the type of media. The small dependency of the oxide layer on the type of media was expected as such a layer is identical for the titanium electrodes in different wells. The R_S was calculated to be 53 ± 6 , 54 ± 22 , 34 ± 2 , 32 ± 2 , and $6 \pm 4 \Omega\cdot\text{cm}^2$ for DI water, HEPES, PBS, RPMI, DMEM, and Fe(II)Fe(III), respectively. The magnitude of R_S followed expectation of being decreased with the increase of ionic strength of the media. To better quantify any possible contribution of protein adsorption to the well impedance, the contribution of serum protein within RPMI media on the temporal impedance data was also evaluated. The results showed no significant difference in either $R_S(R_M)$ or R_{CT} when compared to the

other media.

4.3. Contribution of cell-culture insert to the impedance

The contribution of placing a microporous membrane (insert) to the impedance was evaluated in PBS and compared with the condition of having no insert. The results are reflected in Table 2 and indicates that the presence of the insert (of any pore size) resulted in an increase of around 75% in apparent solution (membrane) resistance, R_S , independent of the membrane pore size of the insert. The porous membrane allows the free transport of fluids between the compartments, however, as the results indicate, the presence of the insert affected the measured apparent solution resistance of the wells (Huang et al., 2018). This is believed to arise from a membrane potential that opposes the streaming of ions through the membrane (Kasianowicz et al., 1996) (Ho et al., 2005).

4.4. Simulation of electric field (EF) distribution within the well

The exploded version of the model used for analysis and response of the system to the application of 50 mV to the top and grounded bottom electrode of a single well are shown in Fig. 4. A steadily decreasing field strength is observed along a line connecting the center of the two electrodes which peaks at the insert as the EF is stronger at the insulator based on Gauss's Law (Fig. 4D). The EF on the membrane, Fig. 4E, shown to be uniform across the membrane's surface confirms the uniformity assumption of EF in the design. The two far 0.5 mm region in the beginning and end of membrane are the edges where the membrane is sealed to the insert. The effect of insert porosity was also evaluated by assigning a weighted average permittivity (simple rule of mixtures) to the membrane based on the permittivity of PET ($\epsilon = 3$) and PBS ($\epsilon = 80$). Fig. 4E show the 2D distribution of EF along a line connecting the center

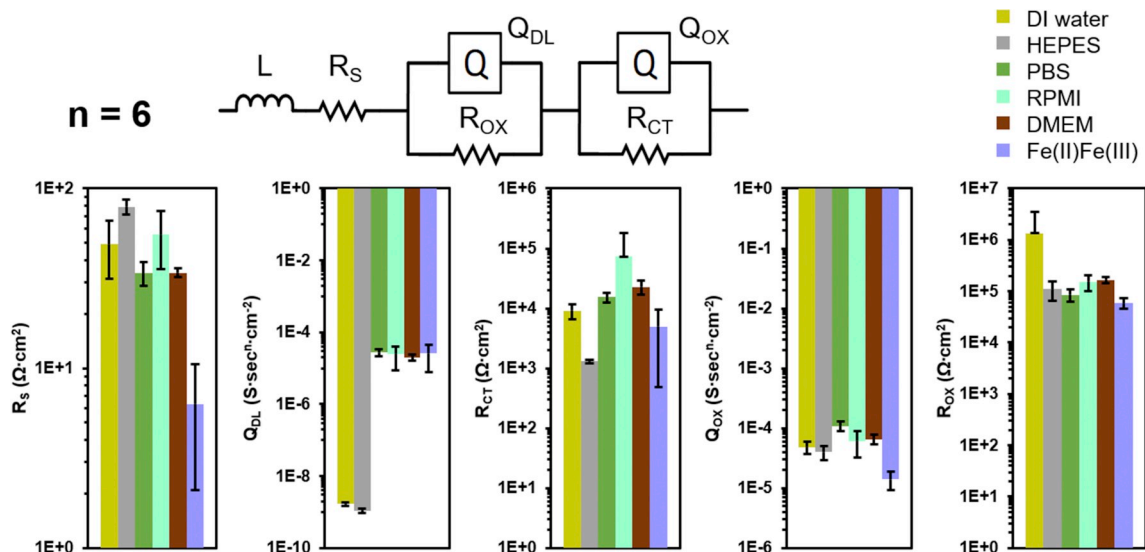


Fig. 3. The results of equivalent circuit analysis of EIS data collected from six different media: DI water, 0.1 M HEPES, 0.01 M PBS, RPMI, DMEM, and Fe(II)/Fe(III) at 37 °C.

Table 2

The effect of the presence of cell culture inserts with membrane pore size of 0.4 and 3 μm on the impedance of electroculture wells containing PBS (n = 3).

	R_S ($\Omega\cdot\text{cm}^2$)
PBS (no insert)	46.4 \pm 0.5
0.4 μm pore size	81.4 \pm 5.3
3.0 μm pore size	79.4 \pm 2.0

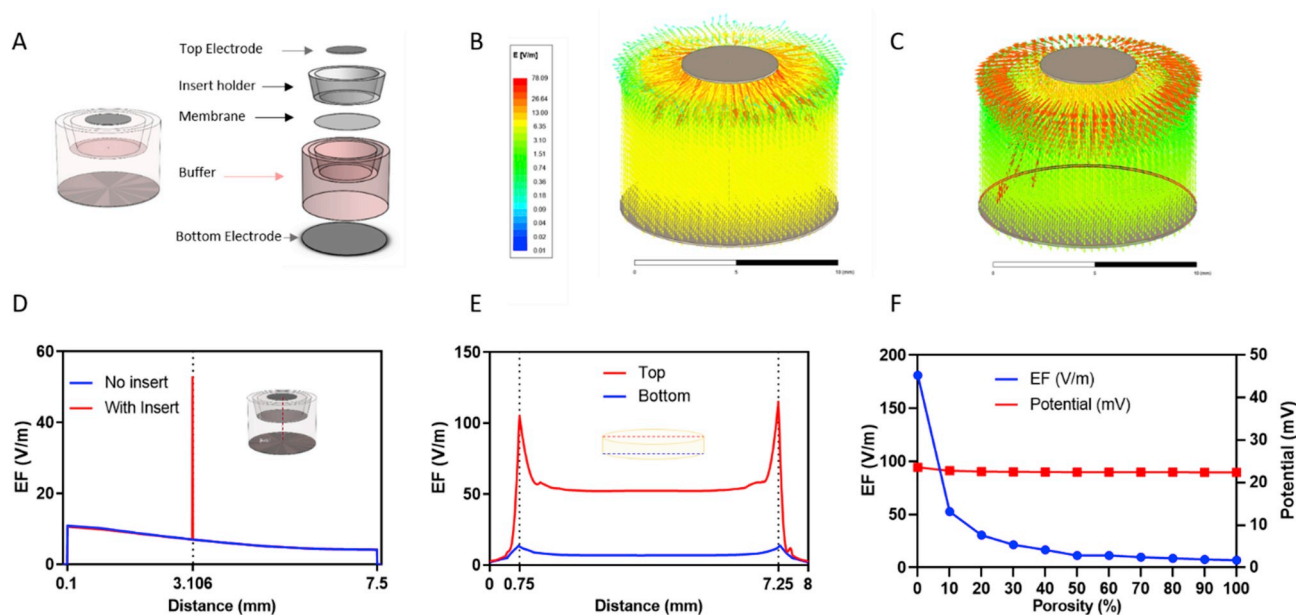


Fig. 4. Electric field distribution within a single well of the 24-well electroculture plate: (A) An exploded view of the well model. The EF distribution between the two electrodes upon application of 50 mV with (B) no insert and (C) an insert of 10% membrane porosity. (D) The EF strength along a line connecting the top and bottom electrode when there is no insert and with insert of 10% porosity. (E) The EF strength along the diameter on the cell-bearing top and bottom surfaces. (F) The magnitude of EF (left) and potential (right) on the membrane ($D = 3.106$ mm) upon application of 50 mV as a function of membrane porosity (0–100%).

of top and bottom electrodes with increasing porosity from 0% (no membrane) to 100% (PET) in 10% increments which shows the uniform EF distribution on the membrane. Fig. 4F shows the EF and potential on top of the membrane as a function of porosity. As shown, the EF on top of membrane depends on the porosity and is highest when the porosity is 0% (pure PET) and decreases as the membrane become more porous. In practice, the porosity of commercially available membrane used in hanging cell culture insert is 10%–15%, therefore the cells do not experience a large difference in EF depending on the membrane porosity.

4.5. EF effect on HUVECs monitored by EIS in ECSARA

According to the viability data presented in Fig. 5A, during the first day, the HUVEC population of EF-stimulated group was smaller than control (0.8 fold), they outnumbered the control after 3 days (1.2 fold) and stayed at that level from day-4 onwards. The data suggest that the growth was initially inhibited by EF stimulation but eventually adapted to support the proliferation of the cells until both test and control cells formed a confluent monolayer at about the fourth day of culture. Temporal changes in the extracted resistance of the cells (R_{cell}) measured over a five-day period are shown in Fig. 5C. The R_{cell} was attributed to the combined presence of HUVECs on the porous membrane of the insert from the EQCRT corresponding to $LR_s(Q_{Cell}R_{Cell})(Q_{OX}R_{OX})(Q_{DL}R_{CT})$. The resistance of EF-stimulated and control cells started to increase at 54 h and 78 h, respectively and reached a constant level at 102 h. The resistance of the monolayer of HUVEC cells, known as TEER, has been vastly used as an indicator of formation of epithelial/endothelial monolayer and formation of tight junctions (Benson et al., 2013). The growth rate of the HUVECs using viability data is shown in Fig. 5B presents the ratio of the absorbance relative to the last time point (previous day) is in accordance with the EIS data where it is shown that EF-stimulated HUVECs reached to higher number/confluency faster than control cells as have been reported previously (Li et al., 2017; Yen-Patton et al., 1988). It is noteworthy that formation of tight junctions, clearly traceable with transmembrane resistance, could be different for different cell numbers since, while the cell population may increase, tight junctions may not form. The optical micrographs taken of

sacrificed insert shows the approach to confluence as the HUVEC layer became established on the insert. The visualization of VE-cadherin, a protein expressed in tight junctions, confirmed that adjacent cells formed tight junctions, which resist ions/molecules transport through the monolayer which reflected in the measured increase in resistance. The effect of EF on endothelial cells has been mostly investigated in terms of orientation and migration of these cells (Li and Kolega, 2002; Zhao et al., 2004), which in the case of the present study, as the plate is not designed to deliver the EF-parallel to the growth plane of the cells, no substantial changes in morphology was observed. The effectiveness of the EF on the expression of angiogenic factors by HUVECs *in-vitro* has been also reported (Geng et al., 2019; Yuan et al., 2014) which shows the effect of FE beyond the morphometric parameters. The effect of shear stress and flow force in microfluidic system (Mathur et al., 2019), inspired by the movement of blood in the vessels, have been vastly investigated and shown to clearly affect HUVECs (Song and Munn, 2011). EF as another type of force, could be compared to such mechanical stimulation. The positive effect of pulsatile signals on angiogenesis at frequencies similar to heart rate (72 beats/min corresponded to 1.2 Hz) (Au et al., 2007; Yuan et al., 2014) could be supportive of the hypothesis of similarity between mechanical and electrical stimulations.

5. Conclusions

Electric field has been named as one of the influential factors in wide variety of phenomena from influencing chemical reactions to altering biological transport phenomena. An electrification system, the ECSARA, for the simultaneous EF stimulation and AC interrogation of cells has been designed, constructed, modeled and tested with HUVECs. The ECSARA offers a true bi-functional platform to study the influence of electrical stimulation and real-time monitoring of the response via EIS. Within the 24-well electroculture well format, a uniform electric field is applied to cells cultured on microporous membranes of cell culture inserts. Stable, reproducible measurement of impedance was demonstrated over a five-day cell culture period. A wide variety of media demonstrate stable performance with solution resistances that match the known ion concentrations and mobilities. ECSARA was used to apply electrical stimulation to HUVECs while monitoring the evolving

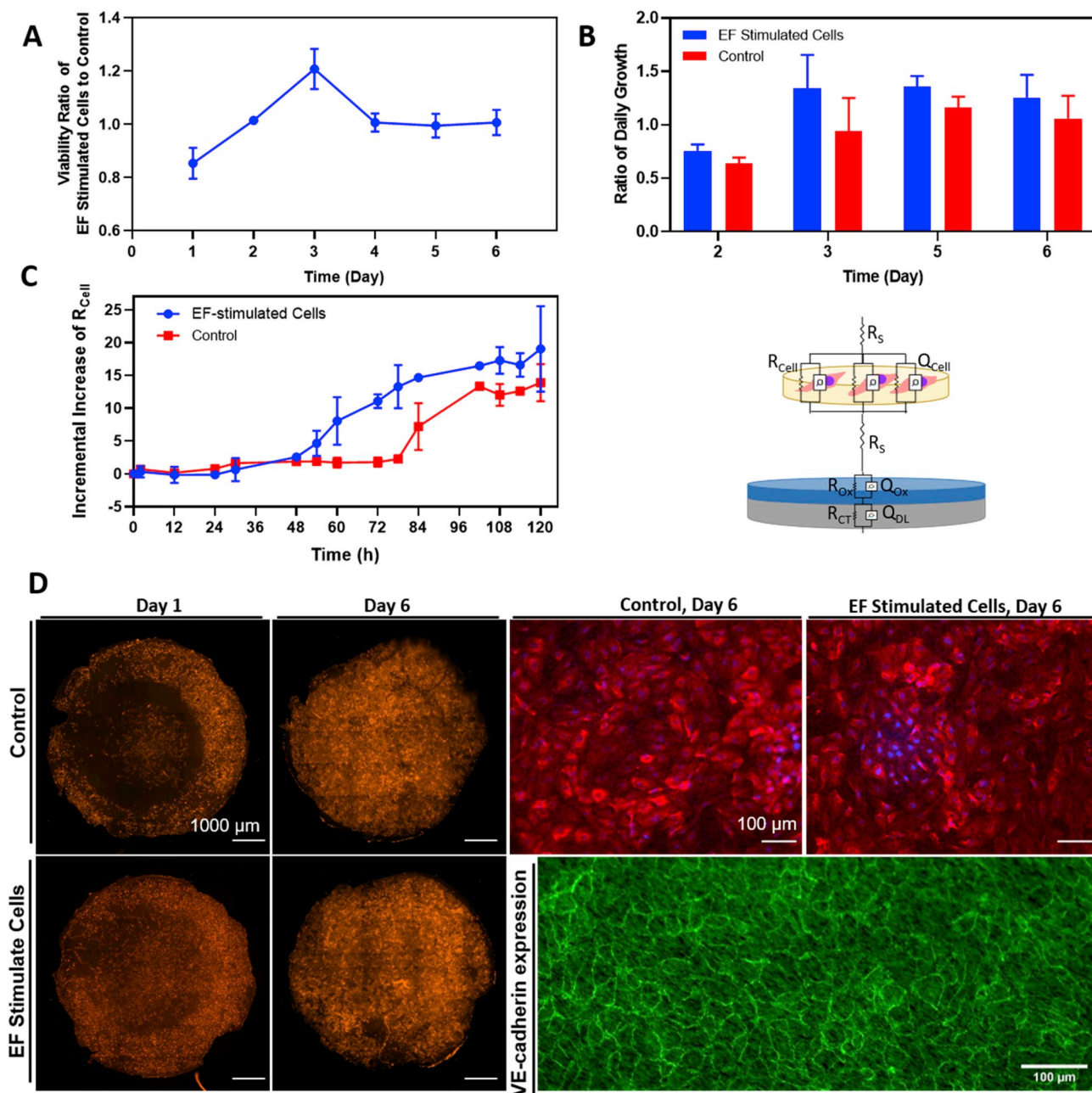


Fig. 5. (A) Ratio of number of EF-stimulated to control cells and (B) ratio of daily population of cells compared to first day obtained from Alamar Blue assay. (C) The changes in the resistance (R_{Cell}) extracted from EIS data and schematic representation of the equivalent circuit elements used in the modeling of TEER. (D) The micrograph of sacrificed insert showing the HUVECs in EF stimulated and control stained for actin filaments (red fluorescent) and DAPI (blue). Evidence of tight junction formation via fluorescent staining of HUVECs with anti VE-cadherin Alexa Fluor® 488. (For interpretation of the references to colour in this figure legend, the reader is referred to the Web version of this article.)

impedance of the cells. The well-known *transepithelial/transendothelial electrical resistance (TEER)* was studied over a six-day period and showed an increase of R_{Cell} as the cells grew to confluence in accordance with data collected from standard Alamar Blue viability assay. The EF showed to reduce the time to confluency of HUVECs. Monitoring R_{Cell} confirmed the suitability of the ECSARA as a real-time monitoring device.

Declaration of competing interest

The authors declare the following financial interests/personal relationships which may be considered as potential competing interests: Prof. Dr. A. G.-E. is founder and scientific director of ABTECH Scientific,

Inc., manufacturer of microfabricated biochip devices. He is a Fulbright Specialist sponsored by the US Department of State through World Learning and has been appointed to University of Tucumán (UT - 2015) and Wrocław University of Science and Technology (WUST - 2019). He has been funded by the Burroughs Wellcome Fund (2019).

CRediT authorship contribution statement

Sara Abasi: Conceptualization, Methodology, Software, Validation, Investigation, Formal analysis, Writing - original draft, Writing - review & editing. **John R. Aggas:** Conceptualization, Software, Validation, Formal analysis, Writing - review & editing. **Naren Venkatesh:** Software. **Iris G. Vallavanatt:** Investigation. **Anthony Guiseppi-Elie:**

Conceptualization, Methodology, Validation, Data curation, Writing - original draft, Writing - review & editing, Visualization, Supervision, Project administration, Funding acquisition, Resources.

Acknowledgments

Support provided by the Center for Bioelectronics, Biosensors, and Biochips (C3B) and from ABTECH Scientific, Inc. Prof. Guiseppi-Elie acknowledges support via a TEES Research Professorship.

Appendix A. Supplementary data

Supplementary data to this article can be found online at <https://doi.org/10.1016/j.bios.2019.111793>.

References

- Abasi, S., Aggas, J.R., Guiseppi-Elie, A., 2019. *Mater. Sci. Eng. C* 99, 1304–1312.
- Adcock, A.F., Agbai, C.O., Yang, L., 2018. *J. Anal. Sci. Technol.* 9 (1), 17.
- Au, H.T.H., Cheng, L., Chowdhury, M.F., Radisic, M., 2007. *Biomaterials* 28 (29), 4277–4293.
- Balint, R., Cassidy, N.J., Cartmell, S.H., 2013. *Tissue Eng. B Rev.* 19 (1), 48–57.
- Benson, K., Cramer, S., Galla, H.-J., 2013. *Fluids Barriers CNS* 10 (1), 5.
- Bieberich, E., Guiseppi-Elie, A., 2004. *Biosens. Bioelectron.* 19 (8), 923–931.
- Brown, M.A., Goel, A., Abbas, Z., 2016. *Angew. Chem. Int. Ed.* 55 (11), 3790–3794.
- Brummer, S.B., Turner, M.J., 1977. *IEEE Trans. Biomed. Eng.* BME 24 (1), 59–63.
- Dellis, J.-L., 2010. *MATLAB. MathWorks, Natick, MA (MathWorks)*.
- du Bois-Reymond, E., 1843. *Ann. Phys.* 134 (1), 1–30.
- Famm, K., Litt, B., Tracey, K.J., Boyden, E.S., Slaoui, M., 2013. *Nature* 496, 159.
- Franks, W., Schenker, I., Schmutz, P., Hierlemann, A., 2005. *IEEE Trans. Biomed. Eng.* 52 (7), 1295–1302.
- Fujita, H., Nedachi, T., Kanzaki, M., 2007. *Exp. Cell Res.* 313 (9), 1853–1865.
- Gan, L., Tan, N.C.S., Gupta, A., Singh, M., Pokholenko, O., Ghosh, A., Zhang, Z., Li, S., Steele, T.W.J., 2019. *Chem. Commun.* 55 (68), 10076–10079.
- Geng, K., Wang, J., Liu, P., Tian, X., Liu, H., Wang, X., Hu, C., Yan, H., 2019. *Am. J. Physiol. Cell Physiol.* 317 (2), C277–C286.
- Giaever, I., Keese, C.R., 1984. *Proc. Natl. Acad. Sci.* 81 (12), 3761–3764.
- Griffin, M., Bayat, A., 2011. *Eplasty* 11 e34–e34.
- Ho, C., Qiao, R., Heng, J.B., Chatterjee, A., Timp, R.J., Aluru, N.R., Timp, G., 2005. *Proc. Natl. Acad. Sci. U.S.A.* 102 (30), 10445–10450.
- Hotary, K.B., Robinson, K.R., 1994. *Dev. Biol.* 166 (2), 789–800.
- Huang, C.Q., Carter, P.M., Shepherd, R.K., 2001. *Ann. Biomed. Eng.* 29 (9), 791–802.
- Huang, Q., Luo, Q., Chen, Z., Yao, L., Fu, P., Lin, Z., 2018. *Environ. Sci.: Water Res. Technol.* 4 (8), 1145–1151.
- Jaffe, L.F., Vanable, J.W., 1984. *Clin. Dermatol.* 2 (3), 34–44.
- Justin, G., Finley, S., Abdur Rahman, A.R., Guiseppi-Elie, A., 2009. *Biomed. Microdevices* 11 (1), 103–115.
- Kasianowicz, J.J., Brandin, E., Branton, D., Deamer, D.W., 1996. *Proc. Natl. Acad. Sci.* 93 (24), 13770–13773.
- Kloth, L.C., 2005. *Int. J. Low. Extrem. Wounds* 4 (1), 23–44.
- Li, X., Kolega, J., 2002. *J. Vasc. Res.* 39 (5), 391–404.
- Li, Y., Li, X., Zhao, R., Wang, C., Qiu, F., Sun, B., Ji, H., Qiu, J., Wang, C., 2017. *Mater. Sci. Eng. C* 72, 106–112.
- Lo, C.-M., Ferrier, J., 1998. *Phys. Rev. E* 57 (6), 6982–6987.
- Lo, C.M., Keese, C.R., Giaever, I., 1995. *Biophys. J.* 69 (6), 2800–2807.
- Mathur, T., Singh, K.A., Pandian, N.K.R., Tsai, S.-H., Hein, T.W., Gaharwar, A.K., Flanagan, J.M., Jain, A., 2019. *Lab Chip* 19 (15), 2500–2511.
- McCaig, C.D., Rajnicek, A.M., Song, B., Zhao, M., 2005. *Physiol. Rev.* 85 (3), 943–978.
- Metcalfe, M.E.M., Borgens, R.B., 1994. *J. Exp. Zool.* 268 (4), 323–338.
- Mobini, S., Leppik, L., Barker, J.H., 2016. *Biotechniques* 60 (2), 95–98.
- Nuccitelli, R., 1992. *Bioelectromagnetics* 13 (S1), 147–157.
- Nuccitelli, R., 2003. *Radiat. Prot. Dosim.* 106 (4), 375–383.
- Ping, J., Gao, F., Chen, J.L., Webster, R.D., Steele, T.W.J., 2015. *Nat. Commun.* 6, 8050.
- Poo, M.-m., Robinson, K.R., 1977. *Nature* 265 (5595), 602–605.
- Robinson, K.R., 1985. *J. Cell Biol.* 101 (6), 2023–2027.
- Song, B., Gu, Y., Pu, J., Reid, B., Zhao, Z., Zhao, M., 2007. *Nat. Protoc.* 2, 1479.
- Song, J.W., Munn, L.L., 2011. *Proc. Natl. Acad. Sci.* 108 (37), 15342–15347.
- Suni, I.I., 2008. *Trac. Trends Anal. Chem.* 27 (7), 604–611.
- Tamilselvi, S., Vedarajan, R., Nallaiyan, R., 2006. *Electrochim. Acta* 53 (3), 839–846. <https://doi.org/10.1016/j.electacta.2006.06.018>.
- Tandon, N., Cannizzaro, C., Figallo, E., Voldman, J., Vunjak-Novakovic, G. (Eds.), 2006. 2006 International Conference of the IEEE Engineering in Medicine and Biology Society, pp. 845–848.
- Tandon, N., Marsano, A., Cannizzaro, C., Voldman, J., Vunjak-Novakovic, G. (Eds.), 2008. 2008 30th Annual International Conference of the IEEE Engineering in Medicine and Biology Society, pp. 3594–3597.
- Vanhaesebroeck, B., 2006. *Nat. Chem. Biol.* 2, 453.
- Wegener, J., Abrams, D., Willenbrink, W., Galla, H.-J., Janshoff, A., 2004. *Biotechniques* 37 (4), 590–597.
- Williams, J.C., Hippensteel, J.A., Dilgen, J., Shain, W., Kipke, D.R., 2007. *J. Neural Eng.* 4 (4), 410–423.
- Xing, J.Z., Zhu, L., Jackson, J.A., Gabos, S., Sun, X.-J., Wang, X.-b., Xu, X., 2005. *Chem. Res. Toxicol.* 18 (2), 154–161.
- Xiong, G.M., Do, A.T., Wang, J.K., Yeoh, C.L., Yeo, K.S., Choong, C., 2015. *J. Biol. Eng.* 9 (1), 14.
- Yamada, M., Tanemura, K., Okada, S., Iwanami, A., Nakamura, M., Mizuno, H., Ozawa, M., Ohyama-Goto, R., Kitamura, N., Kawano, M., Tan-Takeuchi, K., Ohtsuka, C., Miyawaki, A., Takashima, A., Ogawa, M., Toyama, Y., Okano, H., Kondo, T., 2007. *Stem Cells* 25 (3), 562–570.
- Yang, L., Guiseppi-Elie, A., 2008. Impedimetric biosensors for nano- and microfluidics. In: Li, D. (Ed.), *Encyclopedia of Microfluidics and Nanofluidics*. Springer US, Boston, MA, pp. 811–823.
- Yen-Patton, G.P.A., Patton, W.F., Beer, D.M., Jacobson, B.S., 1988. *J. Cell. Physiol.* 134 (1), 37–46.
- Yuan, X., Arkonac, D.E., Chao, P.-h.G., Vunjak-Novakovic, G., 2014. *Sci. Rep.* 4, 3674.
- Zhang, Y.S., Aleman, J., Shin, S.R., Kilic, T., Kim, D., Mousavi Shaegh, S.A., Massa, S., Riahi, R., Chae, S., Hu, N., Avci, H., Zhang, W., Silvestri, A., Sanati Nezhad, A., Manbohi, A., De Ferrari, F., Polini, A., Calzone, G., Shaikh, N., Alerasol, P., Budina, E., Kang, J., Bhise, N., Ribas, J., Pourmand, A., Skardal, A., Shupe, T., Bishop, C.E., Dokmeci, M.R., Atala, A., Khademhosseini, A., 2017. *Proc. Natl. Acad. Sci.* 114 (12), E2293–E2302.
- Zhao, M., 2009. *Semin. Cell Dev. Biol.* 20 (6), 674–682.
- Zhao, M., Bai, H., Wang, E., Forrester, J.V., McCaig, C.D., 2004. *J. Cell Sci.* 117 (3), 397–405.